Geochemistry Geophysics Geosystems G3

Article
Volume 12, Number 10
27 October 2011
Q0AK02, doi:10.1029/2011GC003698
ISSN: 1525-2027

Published by AGU and the Geochemical Society

Viscous coupling at the lithosphere-asthenosphere boundary

Tobias Höink
Department of Earth Science, Rice University, Houston, Texas 77005, USA (tobias.hoeink@rice.edu)

A. Mark Jellinek
Department of Earth and Ocean Sciences, University of British Columbia, Vancouver, British Columbia M5S 1A7, Canada

Adrian Lenardic
Department of Earth Science, Rice University, Houston, Texas 77005, USA

[1] Tectonic plate motions reflect dynamical contributions from subduction processes (i.e., classical "slab-pull" forces) and lateral pressure gradients within the asthenosphere ("asthenosphere-drive" forces), which are distinct from gravity forces exerted by elevated mid-ocean ridges (i.e., classical "ridge-push" forces). Here we use scaling analysis to show that the extent to which asthenosphere-drive contributes to plate motions depends on the lateral dimension of plates and on the relative viscosities and thicknesses of the lithosphere and asthenosphere. Whereas slab-pull forces always govern the motions of plates with a lateral extent greater than the mantle depth, asthenosphere-drive forces can be relatively more important for smaller (shorter wavelength) plates, large relative asthenosphere viscosities or large asthenosphere thicknesses. Published plate velocities, tomographic images and age-binned mean shear wave velocity anomaly data allow us to estimate the relative contributions of slab-pull and asthenosphere-drive forces for the motions of the Atlantic and Pacific plates. Whereas the Pacific plate is driven largely by slab pull, the Atlantic plate is predicted to be strongly driven by basal forces related to viscous coupling to strong asthenospheric flow, consistent with recent observations related to the stress state of North America. In addition, compared to the East Pacific Rise (EPR), the relatively large lateral pressure gradient near the Mid-Atlantic Ridge (MAR) is expected to produce significantly steeper dynamic topography. Thus, the relative importance of this plate-driving force may partly explain why the flanking topography at the EPR is smoother than at the MAR. Our analysis also indicates that this plate-driving force was more significant, and heat loss less efficient, in Earth's hotter past compared with its cooler present state. This type of trend is consistent with thermal history modeling results which require less efficient heat transfer in Earth's past.

Components: 9500 words, 8 figures, 1 table.

Keywords: asthenosphere; lithosphere; plate tectonics; stress coupling; wavelength of convection.

Index Terms: 8120 Tectonophysics: Dynamics of lithosphere and mantle: general (1213); 8149 Tectonophysics: Planetary tectonics (5475).

Received 11 May 2011; **Revised** 31 August 2011; **Accepted** 9 September 2011; **Published** 27 October 2011.

Höink, T., A. M. Jellinek, and A. Lenardic (2011), Viscous coupling at the lithosphere-asthenosphere boundary, *Geochem. Geophys. Geosyst.*, *12*, Q0AK02, doi:10.1029/2011GC003698.

Theme: The Lithosphere-Asthenosphere Boundary
Guest Editors: M. S. Miller, J. B. Gaherty, A. G. Jones. C. P. Conrad, and S. Y. O'Reilly

1. Introduction

[2] Extensive recent work has investigated how the asthenosphere, a sub-lithospheric zone of low viscosity, governs the viscous resistance to plate motions, and, in turn, the wavelength of mantle convection [*Richards et al.*, 2001; *Busse et al.*, 2006; *Lenardic et al.*, 2006; *Höink and Lenardic*, 2008, 2010]. Three-dimensional mantle convection simulations [*Höink and Lenardic*, 2010] show also that buoyancy effects related to lateral temperature variations in the asthenosphere may influence the driving force for plate tectonics under certain conditions. For example, Figure 1a shows a snapshot from a mantle convection simulation in which a cold, high viscosity lithosphere that is subducting at the right side of the box overlies a warm, low-viscosity asthenosphere. Each vertical velocity profile shown can be decomposed into the superposition of a linear velocity gradient related to simple shear imparted to the asthenosphere at the base of the moving lithosphere (i.e., the "Couette flow" component) and a parabolic velocity profile in the asthenosphere associated with the flow driven by lateral temperature variations (i.e., the "Poiseuille flow" component). The downstream evolution of the profiles shows a monotonic reduction in the strength of the Poiseuille component with distance. In particular, over lateral length scales comparable to or less than the mantle depth, flow in the asthenosphere is dominantly of Poiseuille type, which implies the potential for a significant contribution to the observed surface plate velocity. Flow in the asthenosphere can provide a plate driving force acting on the base of the plate, which is distinct from the ridge-push force, in which elevated topography, generated at mid-ocean ridges, is acting on the plate volume. In the limit in which plates are not moving, i.e. the limit of stagnant-lid convection, ridge-push forces cannot exist for the lack of ridges. In contrast, the asthenosphere-drive mechanism is still predicted to exert a force at the base of plate, but at a magnitude too small to overcome the strength of the plate.

[3] Related to the asthenosphere-drive mechanism, but developed independently, *Alvarez* [2010] has proposed a mechanism termed "continental undertow" in which continental plates are driven by basal tractions, explaining protracted continental collisions which lack a driving mechanism associated with slab pull.

[4] Moreover, *Höink and Lenardic* [2010] find two distinct plate motion regimes with a transition that is governed by the nature of the asthenosphere flow and the wavelength of the plate-scale convection (cf. distinct breaks in scaling trends in Figures 1b and 1c). In more detail, they identify a power law relationship between the convective cell aspect ratio and the asthenosphere velocity ratio, i.e. the ratio of pressure-driven velocity component and velocity component due to shear from the overriding lithosphere. The empirical relationship is found to be universal for the system explored numerically in that it holds across the transition from short to long wavelength flow regimes. Here, we use theoretical scaling analysis to investigate how the numerically observed trend across the regime transition might emerge as a result of the viscous coupling between the asthenosphere and lithosphere layers. This analysis is able to predict numerical simulation results. We apply our analysis to make predictions for the leading-order force balances driving the motions of the Atlantic and Pacific plates. We also discuss implications for Earth's thermal history.

2. Lithosphere-Asthenosphere Model

[5] Motivated by first-order observations of oceanic plates (progressive lithosphere thickening with distance from the ridge [e.g., *Parsons and McKenzie*, 1978] and the existence of a low-viscosity asthenosphere [e.g., *Gutenberg*, 1959; *Hager and Richards*, 1989]), we consider a simple lithosphere-asthenosphere model, shown in Figure 2. In this model, the thermal lid thickness, marked by an isotherm, T_L, increases with distance from the ridge, x, as a result of continuous cooling to the surface. The rate of thermal lid thickening decreases away from the ridge. The relatively cold temperatures of the lithosphere lead to an average high viscosity. Underlying the lithosphere is the asthenosphere, a layer of higher temperature and thus lower average viscosity. Dehydration at the ridge generates a column of dehydrated material, h_{dry}, which advances with the plate, leading to an additional viscosity stratification [*Hirth and Kohlstedt*, 1996; *Lee et al.*, 2005]. For the following scaling analysis (beginning in section 4) we define lithosphere and asthenosphere in terms of viscosity, and use average viscosities in lithosphere, μ_L, and asthenosphere, μ_A. We assume that the low viscosity of the asthenosphere is related to its temperature, the concentration of water and the presence of partial melt. The vertical temperature and viscosity variations in the asthenosphere are very small in comparison to the lithosphere. Con-

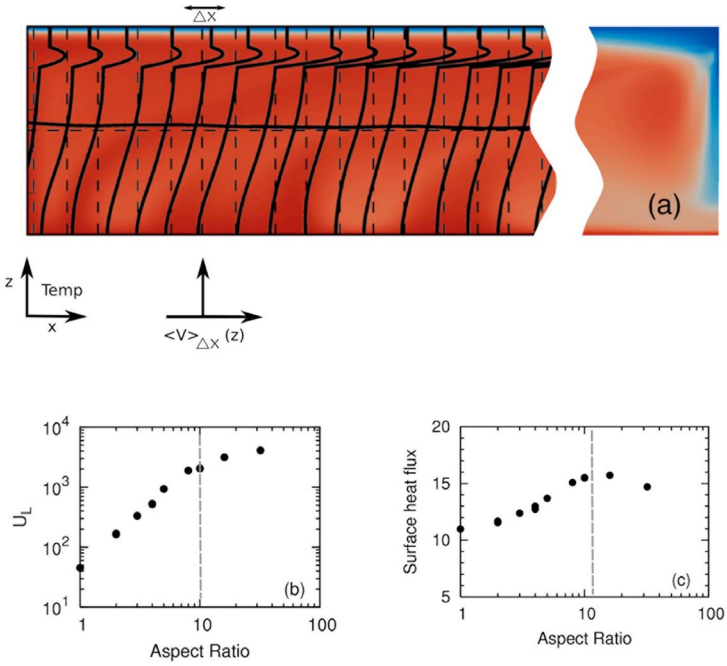

Figure 1. (a) Snapshot of three dimensional mantle convection simulation from *Höink and Lenardic* [2010] with high-viscosity lid (lithosphere analog) and submerged low-viscosity layer (asthenosphere analog) at aspect ratio Γ = 8 in statistically steady state. Shown are temperature side view and horizontal velocity profiles averaged over distances Δx around the dashed lines. Also shown is an averaged vertical velocity profile at mid-depth. A gradual change in asthenosphere flow type occurs as it proceeds downstream. We stress that this flow pattern is not forced by prescribed surface motion; instead it naturally emerges as the most stable flow configuration. (b) Surface velocity versus aspect ratio from numerical simulations show a transition in scaling behavior between short aspect ratio cases and large aspect ratio cases, indicated by dashed line. (c) Surface heat flux versus aspect ratio from numerical simulations show opposing scaling behaviors between short aspect ratio cases and large aspect ratio cases, and a distinct maximum at the transition (indicated by dashed line).

sequently the vertical structure and thickness of the asthenosphere is probably governed by the amount of dissolved water with some contribution from partial melt. Both of these effects are particularly sensitive to pressure and thus we take the asthenosphere to have a relatively flat lower boundary. The thickness of the asthenosphere, h_A, is taken to be approximately constant, which is strictly appropriate at distances greater than h_A from the ridge. For the thickness of the lithosphere we set $h_L = h_{\mathrm{dry}}$.

[6] In this work we define the asthenosphere in terms of relatively low viscosity. Earlier work has investigated different plate models (e.g. "plate model" [*McKenzie*, 1967] and "CHABLIS", in which a constant heat flow is applied to the bottom lithospheric isotherm [*Doin and Fleitout*, 1996]) with respect to how well observations of topography and heat flow can be matched. For the purpose of this paper we do not assume a specific model of thermal lithospheric thickening. The only assumption here is that the thermal lithosphere thickens with distance from the ridge.

[7] A constant surface temperature and progressive thermal lid thickening away from the ridge lead to two opposing flows in the asthenosphere. Whereas lateral differences in hydrostatic pressure (Figure 2b) essentially "squeezes" the asthenospheric material towards the ridge, related lateral temperature variations (Figure 2a) cause relatively cold asthenosphere to spread away from the ridge. Where either mechanism governs the dynamics in the asthenosphere and whether these dynamics influence the overlying plate in a significant way is considered in section 5 below.

[8] In our analysis we consider the lithosphere and asthenosphere system to be a viscously coupled two-layer fluid system where an effectively high-viscosity mechanical lithosphere of depth $h_L(x)$,

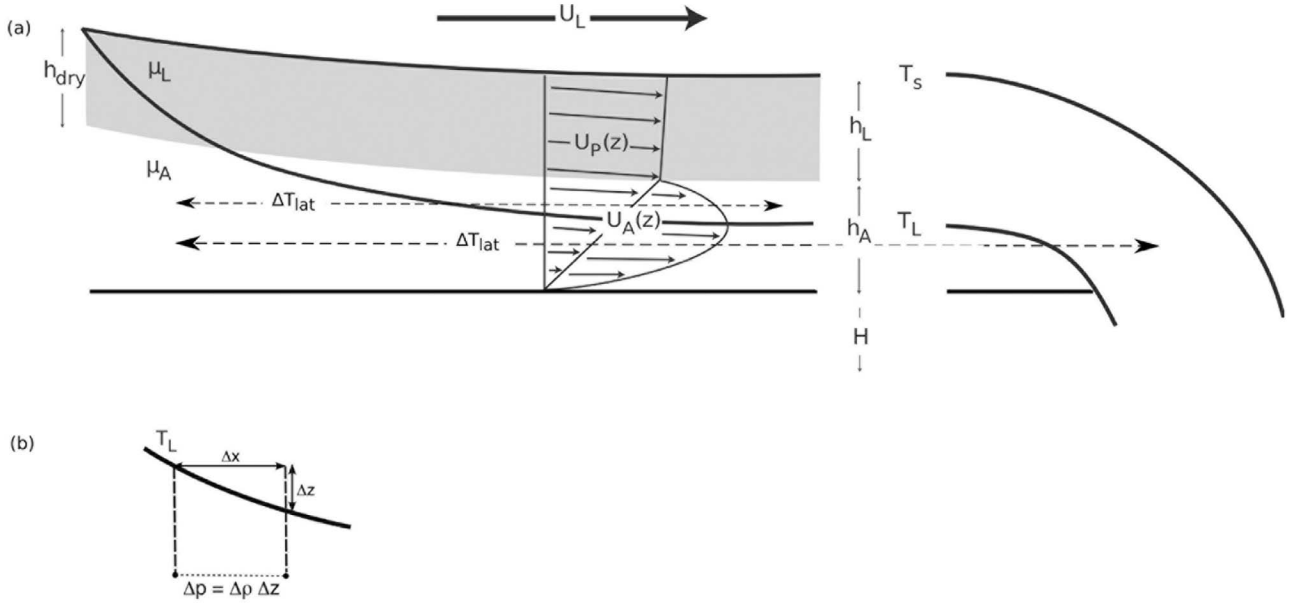

Figure 2. Sketch of the lithosphere-asthenosphere model. (a) Large scale processes lead to lithosphere motion, U_P. The thermal lid thickness increases with distance from the ridge, reaching into the low-viscosity channel that is the asthenosphere. The increasing thermal lid thickness, marked by an isotherm T_L, sets up lateral temperature variations in the asthenosphere, ΔT_{lat}, which affect its density distribution, and which is the source of a lateral pressure gradient. (b) The differences in hydrostatic pressure create a second lateral pressure gradient. Here $\Delta\rho$ is the density difference along Δz between two columns (indicated by thick dashed lines) which are due to temperature differences between colder lithosphere and warmer asthenosphere. Both pressure gradients cause flow in the asthenosphere, U_A. Viscous coupling at the lithosphere-asthenosphere boundary leads to an additional plate driving force, which contributes to the observed plate velocity U_L.

average viscosity μ_L and density ρ_L overlies a low-viscosity asthenosphere of depth h_A, average density ρ_A and viscosity μ_A. Whereas lateral variations in temperature lead to only minor variations in viscosity in the asthenosphere (most of the temperature effect on viscosity occurs in the lithosphere), they are gravitationally unstable and can drive flow.

[9] Viscous coupling across the lithosphere-asthenosphere interface implies that the average motions within one layer will affect the mean velocity of the other layer. Viscous coupling has previously been considered mainly in one direction: Large scale plate motions, driven by the buoyancy-regulated slab-pull force [e.g., *Davies and Richards*, 1992], can shear the asthenosphere. However, for appropriate asthenosphere viscosities and sufficiently large asthenospheric flow velocities viscous coupling at the lithosphere-asthenosphere boundary leads to another plate driving force: asthenosphere-drive. We will discuss the origin of the asthenosphere-drive more fully below, and we will identify the conditions in which this force can enhance plate motions.

3. Asthenosphere-Drive Versus Convective Traction

[10] The concept of convective traction goes back to the 1930's when *Holmes* [1931] suggested the "conveyor belt" hypothesis, in which continents are passive rafts driven by convective flow within Earth's mantle. After the advent of plate tectonics and numerous studies on the causes and mechanics of plate motion [e.g., *Elsasser*, 1967; *McKenzie*, 1969], the idea of convective traction driving plates fell out of favor. *Richter* [1973] concluded that fluid dynamic models of the lithosphere-asthenosphere system are "incapable of generating flows in the asthenosphere that move overlying lithospheric plates by viscous traction". He further concluded that a descending slab provides the dominant plate driving force. Noting that viscous coupling at the base of the plate, depending on the

relative velocity between plate and asthenosphere, can either be driving or resisting plate motion, *Forsyth and Uyeda* [1975] and subsequent workers concluded that the asthenosphere is passive, and convective tractions only resist plate motion. Recently, *Alvarez* [2010] has brought back the potential of tractions driving plate motions. He explained protracted continental collisions on Earth, which lack a driving mechanism associated with the subduction of oceanic plates (i.e., slab pull), by a mechanism named "continental undertow", in which continents move as a result of horizontal traction of the mantle acting on the edges and base of deep continental roots.

[11] The idea of shear tractions driving oceanic plates has on the other hand not been revitalized. Although the possibility is acknowledged [e.g., *Schubert et al.*, 2001] the majority view remains that the asthenosphere resists motion.

[12] Although we build on the concept of shear tractions at the base of the plate, the idea of asthenosphere-drive is conceptually different from this traditional concept of shear tractions: Asthenosphere-drive results from viscous coupling of channelized flow in the asthenosphere to the base of a plate, which is moving slower than flow in the asthenosphere. They key assumptions here are that the asthenosphere is a channel of low viscosity and that flow is strongly channelized (i.e. horizontal mantle flow does not extend below the low-viscosity region of the asthenosphere). This leads to distinctly different predictions than older convective traction ideas. Our treatment of this problem allows us to make specific predictions, such as under which conditions asthenosphere-drive is an important driving force, and how the velocity ratio of plate to asthenosphere depends on the plate length. We also point out that these predictions can be tested against numerical simulations and, as we show in section 8, can be compared with observations on Earth to determine if they are consistent with the observations.

4. Asthenosphere-Drive Versus Ridge-Push

[13] The asthenosphere-drive mechanism is also distinct from the classical ridge-push picture. Ridge-push forces arise in response to gradients in hydrostatic head resulting from elevated topography at mid-ocean ridges [*Forsyth and Uyeda*, 1975]. This force is a body force that acts perpendicular to the strike of the ridge to push the lithosphere away from the ridge. Ridge-push forces are of much smaller magnitude than forces related to the subduction of cold, dense slabs [*McKenzie*, 1969; *Conrad and Lithgow-Bertelloni*, 2002].

[14] In contrast, the asthenosphere-drive force is a surface force acting on the base of plate. It results from lateral temperature gradients that lead, in turn, to lateral gradients in hydrostatic pressure that drive flow in the asthenosphere. When asthenospheric flow velocities exceed plate velocities, viscous drag imparted at the asthenosphere-lithosphere boundary acts to draw the plate in the direction of this flow. We note that asthenosphere-drive is only a driving force when flow velocities below the plate exceed plate velocities, and we discuss the conditions for this to occur below.

[15] The qualitative difference between asthenosphere-drive and ridge-push leads to a new class of predictions. In particularly, in contrast to ridge-push, which assumes that topographic differences are isostatically balanced at depth, asthenosphere-drive predicts that topographic differences are balanced by dynamic contributions from pressure gradients that exist in the asthenosphere. How these dynamic contributions can explain the observed difference of mid-ocean ridge topography is discussed in section 8.4.

5. Stress Coupling Between Lithosphere and Asthenosphere

[16] The surface layer velocity can be written as

$$U_L = U_P + U_D \tag{1}$$

where the "plate component" U_P is the contribution to the plate velocity from the slab-pull force and U_D is the velocity component resulting from the asthenosphere-drive force. At very high Rayleigh number ($Ra > 10^6$) heat transfer is approximately independent of the layer depth [*Moore*, 2008]. In this case, the sinking velocity of a drip such as the cold plume shown at the right side of Figure 1 is close to that of a discrete thermal [cf. *Griffiths*, 1986] and is proportional to $Ra_m^{1/3}$ [*Turner*, 1979; *O'Neill et al.*, 2007]. Following standard boundary layer assumptions we assume that the surface velocity scales as the sinking velocity [e.g., *Turcotte and Oxburgh*, 1967; *Jellinek and Manga*, 2004, and references therein]. The scaling for the plate component is then

$$U_P \sim \frac{\kappa}{H} Ra_m^{1/3} \tag{2}$$

where κ is thermal diffusivity, H is the depth of the convecting system (e.g. the mantle in Earth's terms), Ra_m is the mantle Rayleigh number.

[17] In the simulations by *Höink and Lenardic* [2010], lateral flow within the asthenosphere is, in part, a response to lateral temperature variations ΔT_{lat}, arising as a result of a constant surface temperature and increasing lithosphere thickness away from a ridge in proportion to the square root of age (Figure 2c). These lateral temperature variations give rise to density differences and, in turn, to gradients in hydrostatic pressure that drive flow away from the ridge. The strength of this flow depends on the magnitude of the buoyancy force, which can be expressed in terms an effective gravitational acceleration

$$g'_{T_{lat}} = g\,\alpha\,\Delta T_{lat}, \tag{3}$$

where g is the acceleration due to gravity, α is the thermal expansion coefficient and ΔT_{lat} is the scale of lateral temperature variations (Figure 2c). We note that in the Earth these lateral temperature variations may be enhanced locally by the spreading of plume material [*Morgan and Smith*, 1992; *Morgan et al.*, 1995; *Gaherty*, 2001], and thus our models will give, on average, a lower bound on the magnitude of these buoyancy effects.

[18] The increasing lithosphere thickness with age also depresses and "squeezes" the asthenosphere, resulting in an additional, but opposing, pressure gradient, the so-called "lubrication pressure" [e.g., *Joseph*, 1980]. If the thermal lithosphere thickens proportionally with square-root of plate age (Figure 2b) until it flattens out between 20 Ma [*Stein and Stein*, 1994] and 80 Ma [*Parsons and Sclater*, 1977], it scales with distance from the ridge, L, as $dh_L/dL \sim \frac{1}{2}\sqrt{\kappa/U_P L}$, where κ is the thermal diffusion coefficient. Lithosphere thickening produces a lateral pressure gradient $dp/dx = g'_{topo}\,\rho_A\,dh_L/dL$, where g'_{topo} is the effective gravitational acceleration and ρ_A is the average asthenosphere density, which generates asthenosphere flow according to $\mu_A U_A/h_A^2 = dp/dx$. The gravitational acceleration from this effect scales as

$$g'_{topo} \sim 2\,\frac{\mu_A\,U_A}{\rho_A\,h_A^2}\,\sqrt{\frac{U_P L}{\kappa}}. \tag{4}$$

[19] For reasonable physical and geometric conditions [e.g., *Parsons and McKenzie*, 1978; *Hillier and Watts*, 2004] (g = 10 m/s^2, $\alpha = 5 \times 10^5$K^{-1}, $\Delta T_{lat} \sim 100$ K, $\mu_A = 10^{19}$Pa s, ρ_A = 3300 kg/m^3, $\kappa = 10^{-6}$m^2/s, h_A = 70 km, $U_A \sim U_P \sim 1$ cm/a) and assuming that h_A is approximately constant at distances of order h_A away from the ridge, we determine from (3) and (4) that the two gravitational accelerations, or pressure gradients, become comparable in magnitude at length scales (L) larger than 50,000 km (i.e., greater than the Earth's circumference). This demonstrates that the effect of temperature variations is generally more important for the dynamics of the asthenosphere.

[20] Assuming $L \geq H$ an appropriate scale for the spreading rate for the gravity current that originates from lateral temperature variations is

$$U_A \sim \frac{g'_{T_{lat}} h_A^3}{L\nu_A} \tag{5}$$

where $\nu_A = \mu_A/\rho$ is the kinematic viscosity of the bottom layer. To characterize the strength of this flow it will be useful to introduce an asthenosphere Rayleigh number as

$$Ra_A = \frac{g' h_A^3}{\kappa\nu_A}. \tag{6}$$

[21] Whether flow in the asthenosphere can influence plate motions depends critically on the extent of the viscous coupling between them. Continuity of viscous stresses at the asthenosphere-lithosphere interface demands that

$$\mu_L \frac{U_D}{h_L} \sim \mu_A \frac{U_A}{h_A}. \tag{7}$$

Combining (6) and (7) leads to

$$U_D \sim \left(\frac{\kappa}{L}\right)\left(\frac{\mu_A}{\mu_L}\right)\left(\frac{h_L}{h_A}\right) Ra_A. \tag{8}$$

[22] The relative contributions of drag and plate components to the observed surface velocity are given by the lithosphere velocity ratio

$$\frac{U_D}{U_P} \sim \left(\frac{1}{\Gamma}\right)\left(\frac{\mu_A}{\mu_L}\right)\left(\frac{h_L}{h_A}\right)\left(\frac{Ra_A}{Ra_m^{1/3}}\right) \tag{9}$$

where $\Gamma = L/H$ is the aspect ratio and only the dependence on mantle Rayleigh number Ra_m remains to be identified.

6. Characteristic Length Scale

[23] We start by recognizing that the Rayleigh number is foremost defined as a ratio of two time scales, i.e. the ratio of characteristic times for diffusive to advective heat transfer across a scale

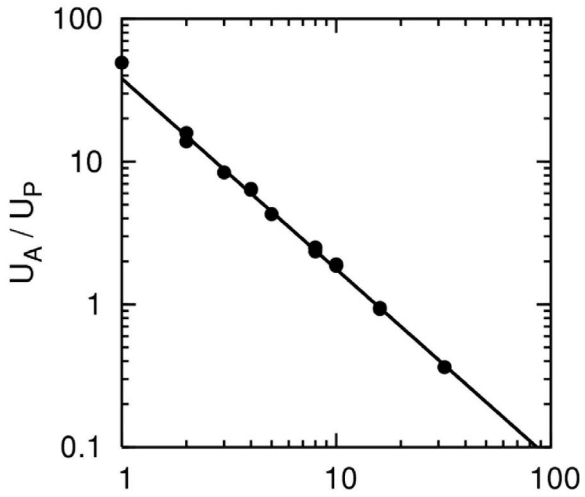

Figure 3. Ratio of velocity components U_A/U_P versus aspect ratio of convection cell. Data points from three-dimensional simulations with different convection cell sizes, Γ, by *Höink and Lenardic* [2010] show that the ratio of pressure-driven flow component to shear driven flow component in the asthenosphere depends on the length of the convection cell in form of a single −4/3-scaling relation.

length. In our model of the lithosphere-asthenosphere system (see Figure 2) the convection cell length L is a natural choice for a characteristic length scale when $L \geq H$ since we are concerned with lateral heat transport. Moreover, such a choice is appropriate in any convecting system in which the wavelength of the flow substantially exceeds the layer depth.

[24] With time scales for diffusion and advection

$$\tau_{diff} = \frac{L^2}{\kappa}, \qquad \tau_{adv} = \frac{L}{U_P}, \tag{10}$$

the mantle Rayleigh number is

$$Ra_m = \frac{U_P}{\kappa} L \tag{11}$$

from which the velocity ratio in the surface layer (equation (9)) follows

$$\frac{U_D}{U_P} \sim \left(\frac{\kappa H}{U_P}\right)^{1/3} \left(\frac{\mu_A}{\mu_L}\right) \left(\frac{h_L}{h_A}\right) Ra_A \Gamma^{-2/3} \tag{12}$$

[25] We note that the theory assumes a channel of low viscosity ($\mu_A \ll \mu_L$)and finite thickness ($h_A > 0$), consistent with many observations and inferences [*Gutenberg*, 1959; *Hager and Richards*, 1989; *Thoraval and Richards*, 1997; *Paulson and Richards*, 2009]. Further it will break down if $\mu_A/\mu_L \approx 1$, because the whole notion of a channelized flow disappears.

[26] Before we apply this approach to a specific example we will take a closer look at equation (12) in the context of lithosphere and asthenosphere. The lithosphere velocity ratio U_D/U_P tends towards zero in the limits of vanishing asthenosphere viscosity ($\mu_A/\mu_L \ll 1$) or very large asthenosphere thickness ($h_A/h_L \gg 1$). This end-member characterizes the classic picture of a top-driven lithosphere. The other end-member is a bottom-driven lithosphere, i.e. a case where the lithosphere is dragged by the underlying asthenosphere, and the lithosphere velocity ratio is much larger than one ($U_D/U_P \gg 1$). This regime can exist for sufficiently small aspect ratios (small L/H), or for a thick asthenosphere (the buoyancy force scales with h_A^3). The transition between those two regimes, between plate driven lithosphere and asthenosphere-driven lithosphere, should occur around $U_D/U_P \approx 1$ and can be estimated with equation (12).

7. Ratio of Asthenosphere Velocity Components

[27] We will now show how the scaling in equation (12) relates to results from three-dimensional mantle convection simulations [*Höink and Lenardic*, 2010]. An example is given in Figure 1a. Velocity profiles indicate a gradual change in asthenospheric flow type from Poiseuille to Couette flow in the downstream direction, indicating a change in the ratio of pressure-driven velocity component U_A and velocity component due to shear from the overriding lithosphere U_P.

[28] The asthenosphere velocity ratio U_A/U_P scaling can be related to the previously derived lithosphere velocity ratio scaling (equation (12)) by considering equation (5) together with the stress coupling of lithosphere and asthenosphere (equation (7)). The resulting scaling of asthenosphere velocity ratio with aspect ratio,

$$\frac{U_A}{U_P} \sim \left(\frac{\kappa H}{U}\right)^{1/3} Ra_A \, \Gamma^{-4/3}, \tag{13}$$

is shown in Figure 3.

[29] Equation (13) predicts to a very good degree the relation between the ratio of pressure-driven to shear-driven flow versus convective aspect ratio as observed in the numerical simulations by *Höink and Lenardic* [2010].

[30] Both our scaling analysis and numerical simulations show that, with everything else being the same, lower asthenosphere velocity ratios, i.e. larger shear-driven flow components, occur in larger aspect ratio convection cells whereas higher asthenosphere velocity ratios, i.e. larger pressure-driven flow components, occur in smaller aspect ratio convection cells.

[31] The transition aspect ratio, i.e. the aspect ratio at which $U_A/U_D = 1$, depends also on the asthenosphere viscosity, which enters equation (13) via Ra_A. Setting $U_A/U_P = 1$, noting that $\mu_A = \nu_A/\rho_A$, and applying (3) to (13) leads to a relation between asthenosphere viscosity and transition aspect ratio

$$\Gamma_{tr} \propto \mu_A^{-3/4}, \tag{14}$$

which predicts that the transition aspect ratio should shift to smaller aspect ratios with increasing asthenosphere viscosity. For example, an increase of asthenosphere viscosity by a factor of 10 should result in a transition aspect ratio shift by a factor of 0.2. Recent simulations by *Höink and Lenardic* [2010] have shown that a ten-fold asthenosphere viscosity increase does indeed lead to a reduced transition aspect ratio by around 35%, consistent with (14).

8. Discussion

8.1. General Implications for Forces Driving Plates

[32] Velocities of both lithosphere and asthenosphere can be decomposed into contributions from classical "slab-pull" forces and from buoyancy-driven Poiseuille flow in the asthenosphere (asthenosphere-drive), which is not to be confused with 'ridge-push' as discussed above. We have shown by scaling analysis that the ratio of these velocity contributions depends on relative thickness and viscosity of lithosphere and asthenosphere and on the wavelength of the plate-scale convection.

[33] Our scaling analysis explains earlier results [*Höink and Lenardic*, 2010], which identified an empirical power law relationship between velocity ratio and aspect ratio, that captures the slab-pull and asthenospheric drive end-member regimes. Our analysis also elucidates the parameter combination that lead to the transition between these flows. The regime transition occurs when both velocity contributions are of the same order of magnitude, and we provide a formula for its prediction.

[34] Whereas classical slab pull is favored for long plates ($L/H \gg 1$) and very large viscosity variations, the asthenosphere-drive force is favored for shorter plates and smaller viscosity variations. The basic conditions for this driving force are viscous coupling at the lithosphere-asthenosphere boundary and flow in the asthenosphere faster than the plate speed. We note that these conditions are also met in the limit of zero plate velocity, i.e. stagnant-lid convection, which implies that the mechanism of asthenosphere-drive also exists in stagnant-lid convection, even though the magnitude of resulting stresses are too low to break or advance the plate. In contrast, ridge-push forces do not exist in the stagnant-lid limit, which further emphasizes the fundamental difference between ridge-push and asthenosphere-drive.

[35] The significance of this result for Earth is the implication that a plate-driving force other than slab-pull or ridge-push will enter the dynamics governing the motions of small (i.e., "short-wavelength") plates. By contrast, for plate scales much larger than the mantle depth (i.e., "long-wavelength" plates), the Poiseuille component is negligible and plate velocities are consistent with well-established theories for the slab-pull driving forces for plate tectonics [e.g., *Richter and McKenzie*, 1978].

[36] Asthenosphere-drive is related to (but developed independently from) "continental undertow", a recently proposed force to drive continued continental collisions in the absence of slab-pull forces [*Alvarez*, 2010].

[37] The asthenosphere-drive force for oceanic plates is pertinent to recent discussions based on observed subsidence data that suggests the need for a mechanism other than slab-pull or ridge-push [*Adam and Vidal*, 2010; *Croon et al.*, 2011; *Adam and Vidal*, 2011]. The fact that recent data based studies are highlighting the need for plate driving forces beyond classic slab-pull and ridge-push demonstrates that, although the kinematics of plate tectonics are reasonably well understood, unraveling the dynamics of plate tectonics remains an active area of research. Classic plate driving forces are in particular unable to explain first-order observations such as mid-ocean ridge topography, the stress state of North America and, when considered through geologic time, the thermal history of the Earth. We will consider in turn how each of these issues demand a mechanism such as asthenosphere-drive.

8.2. Applications to the Pacific and Atlantic Plates

[38] The Pacific plate is the largest oceanic plate on Earth today with a spatial extent that exceeds the mantle depth and a fast half-spreading rate at the East Pacific Rice (EPR) of about 10 cm/yr. The Pacific plate is conventionally taken to be a canonical example of a slab-driven oceanic plate. Qualitatively, our results do not dispute this basic dynamical picture. In contrast, the Atlantic plate, about a third or less the size of the Pacific plate, spreads to either side of the Mid-Atlantic Ridge (MAR) at about 1 cm/yr. We use the term Atlantic plate to denote the oceanic parts of the North American, South American, European and African plates. The Atlantic plate does not subduct (MAR spreading is accommodated as neighboring plates drifting apart).

[39] To apply our results to understand these particular settings quantitatively we use constraints from seismic tomography to estimate velocity ratios for Pacific plate and Atlantic plate as well as the average thickness of the asthenosphere [*Priestley and McKenzie*, 2006; *Gaherty and Dunn*, 2007]. Both sources provide age-binned shear wave velocities (reproduced in Figure 4), and we estimate a shear wave velocity gradient by converting seafloor age to distance using the half-spreading rates mentioned above. Assuming that variations in mean seismic shear velocity are entirely due to temperature, we use the partial derivative of $\partial \ln V_s/\partial T = -2.1\%/100$ K [*Cammarano et al.*, 2003] to estimate lateral temperature gradients in the asthenosphere (see Appendix A for details).

[40] Taking the asthenosphere thickness and viscosity to be 70 km and 10^{19} Pa s, and from Figure 4 lateral temperature gradients of 7 K/100 km and 50 K/100 km for the Pacific and Atlantic, we can use equations (3), (6) and (13) to estimate a velocity ratio U_A/U_P of order 0.7 underneath the Pacific plate and of order 100 underneath the Atlantic plate. From equation (5), estimates of thickness and viscosity of the asthenosphere influence the derived asthenosphere velocity. Figure 5 shows the dependence of these model parameters, and allows a quick visual quantification of their influence within the range of reasonable parameters. Figure 5 also demonstrates that, for given asthenosphere viscosity and thickness, the predicted velocities in the asthenosphere underneath the Atlantic are almost one order of magnitude larger than those underneath the Pacific.

[41] Together with inferences from seismological observations, our scaling suggests that the asthenosphere underneath the oceanic part of the Atlantic plate is primarily driven by lateral pressure gradients, without significant contribution from large scale convection processes involving the overriding plate, such as "ridge push". In contrast, asthenosphere flow underneath the Pacific plate is mostly driven by shear transmitted across the lithosphere-asthenosphere boundary with minor contributions from pressure-driven flow. We note that this prediction does not take into consideration potential contributions from localized and potentially large intra-plate hot spots sources, such as those creating Hawaiian islands [*Yamamoto et al.*, 2007a, 2007b].

[42] Because asthenosphere and lithosphere are coupled by viscous stresses we can use the asthenosphere velocity ratio and equation (7) to compute the lithosphere velocity ratio, U_D/U_L, which quantifies the contribution of asthenospheric drive to the observed plate speed. For a viscosity ratio between asthenosphere and lithosphere $\mu_A/\mu_L = 0.01$ we predict lithosphere velocity ratio $U_D/U_L \approx 1\%$ for the Pacific plate and $U_D/U_L \approx 70\%$ for the Atlantic plate. While the absolute values depend on the assumed viscosity ratio, the strong difference of two orders of magnitude between the two end-member regimes is independent of the assumed viscosity ratio. The lithosphere velocity ratios suggests that on average the Pacific plate is insignificantly influenced by viscous coupling to flow in the asthenosphere, confirming the traditional perspective of a subduction-driven Pacific plate. This view, however, does not hold for the Atlantic plate, which we predict to be largely driven by viscous coupling to the much faster flowing asthenosphere.

[43] The stress imparted by the sub-Atlantic asthenosphere onto the base of the lithosphere can be estimated as

$$\sigma \sim \eta_L \dot{\epsilon} \sim \eta_L \frac{U_D}{h_L}, \qquad (15)$$

where η_L is the lithosphere viscosity, h_L the plate thickness and $\dot{\epsilon}$ the strain rate. Another approach to select the vertical length scale (replacing h_L) would choosing the length scale for deformation in the lithosphere based on the rheological temperature scale. To first order, due to the strong temperature dependence of viscosity, these length scales can be considered the same.

[44] With order of magnitude values for viscosity (10^{21} Pa s), drag-component of plate velocity

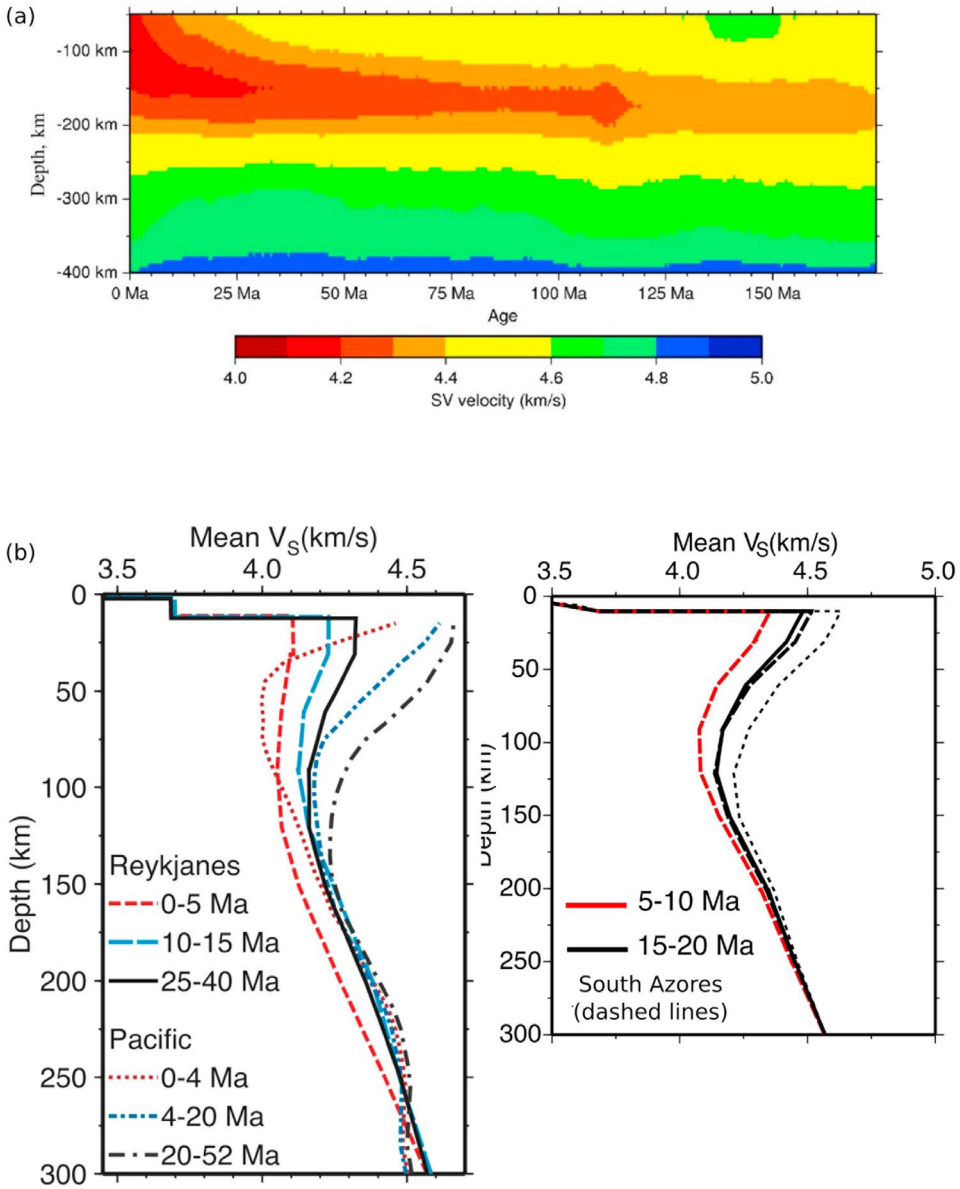

Figure 4. (a) Shear wave velocity beneath the Pacific Ocean (reproduced from *Priestley and McKenzie* [2006], copyright 2006, with permission from Elsevier). (b) Mean shear wave velocity derived (left) from the Pacific (from *Gaherty* [2001]; reprinted with permission from AAAS) and (right) from the South Azores ridge region (reproduced from *Gaherty and Dunn* [2007]). By converting seafloor age to distance, assuming that variations in mean seismic shear velocity are entirely due to temperature, and using the partial derivative of $\partial \ln V_s/\partial T = -2.1\%/100\text{K}$ [*Cammarano et al.*, 2003] we estimate lateral temperature gradients in the asthenosphere to 50 K/100 km (Atlantic) and 7 K/100 km (Pacific).

(0.7 cm/yr) and lithosphere thickness (100 km) we estimate the stress contribution of the Atlantic plate from the underlying asthenosphere to be of order 2 MPa. This value is about an order of magnitude short of tensile rock strengths [*Afrouz*, 1992], which suggests a potential for aseismic deformation, consistent with the observed lack of seismicity where the oceanic Atlantic plate meets the North American continent. The westward stress contribution from the oceanic Atlantic plate in concert with the eastward stress component related to the subducting Pacific plate mostly explains the observed state of compression of much of North America [*Humphreys and Coblentz*, 2007].

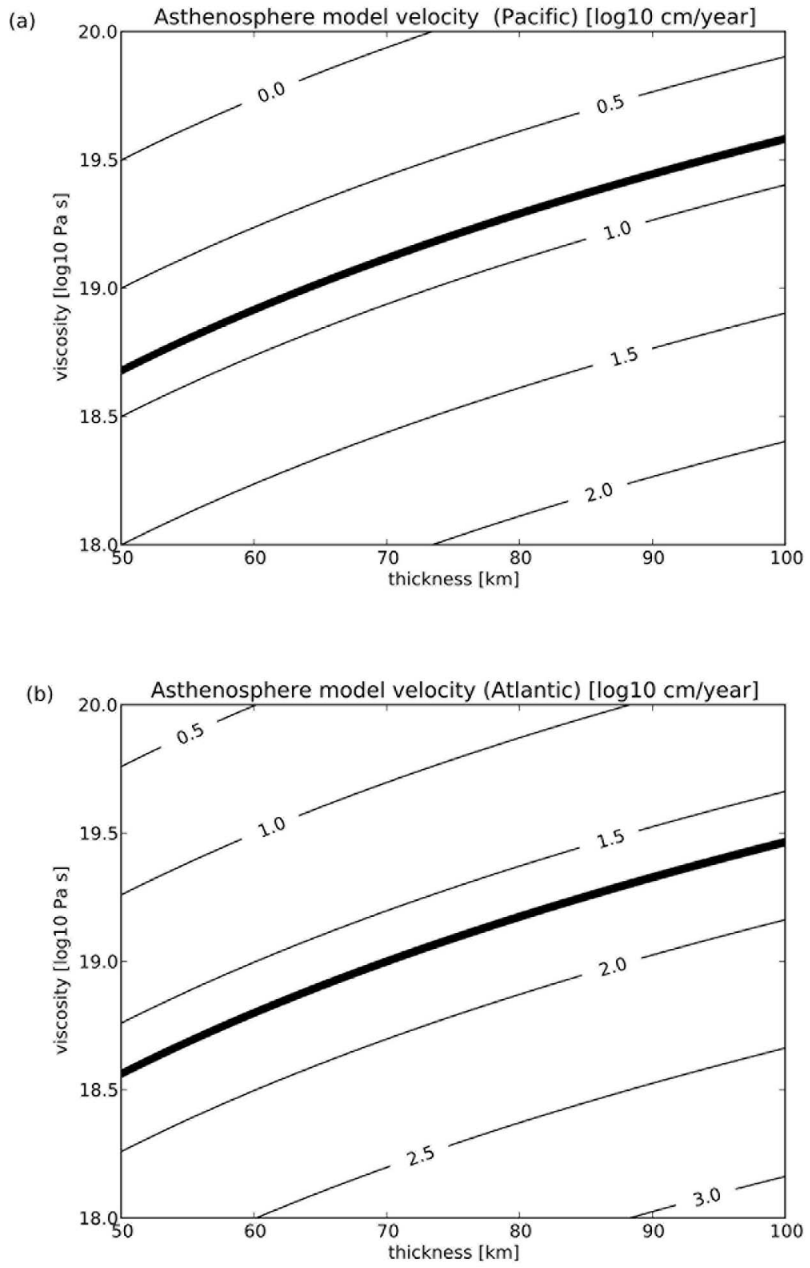

Figure 5. Influence of asthenosphere thickness and viscosity on the modeled flow velocity from pressure-driven flow in the asthenosphere. Thick lines denote the asthenosphere flow velocities of (a) 6.6 cm/year (Pacific) and (b) 50 cm/year (Atlantic) inferred from age-binned seismic shear wave velocities.

8.3. Implications for Asthenosphere Properties

[45] We note that stress transmission from the asthenosphere to the overlying plate requires fast asthenosphere flow relative to the plate, such that the velocity gradient at the base of the plate is positive. This is readily accomplished by channelized flow in a low-viscosity medium and relatively slow plates. For flow channelization to occur the asthenosphere viscosity has to be at least one order of magnitude less than that of the mantle below ($\mu_A < 0.1\ \mu_m$). The low bulk viscosity of the asthenosphere is directly influenced by volatiles (eg. H_2O and CO_2). H_2O can be incorporated into the rock matrix. Estimates suggest a viscosity difference of a factor of 4 between 50 ppm H_2O and saturated conditions [*Dixon et al.*, 2004]. H_2O is also known to lower the melting temperature, but it has been

shown to generate large melt fractions only at temperatures close to the dry solidus [*Hirschmann et al.*, 1999]. Carbon on the other hand is not readily incorporated into the melt, but is thought to generate fractional melt as well [*Dasgupta and Hirschmann*, 2010]. Entrained partial melt may affect bulk properties, including viscosity, and the combined effects of water and melt alone can change the average viscosity by as much as 3 orders of magnitude [*Mei et al.*, 1999; *Scott and Kohlstedt*, 2006]. The viscosity constraint from asthenosphere-drive has therefore the potential to provide insight into the minimum concentration of volatiles within the oceanic asthenosphere.

8.4. Implications for Mid-Ocean Ridge Topography

[46] We now consider how pressure gradients from asthenosphere flow effect observed topography gradients. The lateral pressure gradient in the asthenosphere is $dp/dx \sim \Delta\rho g h_t/L$, where h_t is the topographic height. Since flow in the asthenosphere scales as $U_A \sim -\mu_A^{-1} h_A^2 dp/dx$, the topographic gradient scales as

$$\frac{h_t}{L} \sim \frac{\mu_A U_A}{\Delta\rho g h_A^2}. \tag{16}$$

We note that the topographic gradient is governed by a balance between pressure and viscous stress, and shows an inversely quadratic dependence on asthenosphere thickness h_A. In the current context we assume no significant variations of asthenosphere thicknesses. Instead we focus on the previously introduced strong variation in asthenosphere velocity between the two end-members Pacific and Atlantic. Equation (16) predicts that large asthenosphere flow velocities should lead to a steeper topography gradient than small asthenosphere flow velocities. This connection, in concert with our estimates of relatively slow asthenosphere flow velocities for the Pacific and relatively fast asthenosphere flow velocities for the Atlantic, explains the long-standing observation [e.g., *Lin and Parmentier*, 1989; *Small*, 1994] that the East Pacific Rise shows a smoother flanking topography than the Mid Atlantic Ridge.

[47] The dynamically balanced (i.e. balanced by lateral pressure differences) topography supported by asthenospheric flow is in contrast to the isostatic balance assumption inherent to the ridge-push mechanism (see section 4), which is unable to explain the observed topographic differences.

[48] Throughout this paper we have considered the Pacific plate as a large plate end-member. The present model predicts that large plates that are dominantly driven by slab pull forces lead the asthenosphere (ie. asthenospheric flow is slower than plate velocity). In contrast, for small plates for which a dominant slab-pull is absent, such as the Atlantic plate, asthenosphere-drive is a significant driving force. Our model also predicts for the long-plate limit that flow in the asthenosphere is in part due to shear from the overriding plate and in part due to pressure-gradients, the latter being the same mechanism that is responsible for asthenosphere-drive. However, because the plate is leading, asthenosphere flow below the plate cannot drive the plate. In this limit it might be more appropriate to refer to asthenosphere flow lubricating the plate, thus enhancing motion. The magnitude of this mechanism depends on velocity gradients and viscosity in the asthenosphere. One of our model predictions is that - for all plate lengths - asthenosphere flow depends on plate-length (equation (13)). Because asthenosphere flow relative to the plate decreases in magnitude with increasing plate length, the prediction for the long plate limit is that lubrication decreases with plate length.

[49] In a recent study of subsidence observations [*Adam and Vidal*, 2010] query the Pacific plate across several segments of different length. They conclude that subsidence rate increases with decreasing segment length. We can identify segments of different lengths with different aspect ratios in our analysis under the assumption that transform faults provide a mechanism to decouple plate segments of different lengths. The study by *Adam and Vidal* [2010] agrees qualitatively with our prediction that smaller aspect ratios lead to faster flow in the asthenosphere (Figure 3), and in turn to larger topographic differences.

8.5. Implications for the Mantle Heat Flux Through Time

[50] Our results support the notion that on present day Earth both end-member regimes exist spatially. The Pacific plate overlies a relatively slow asthenosphere, which corresponds to classic mobile-lid convection, while the Atlantic plate overlies a relative fast asthenosphere, representing sluggish-lid convection.

[51] This has important implications regarding planetary scale heat loss and the thermal evolution of our planet. *Höink and Lenardic* [2010] show a distinct break in surface heat flux scaling behavior

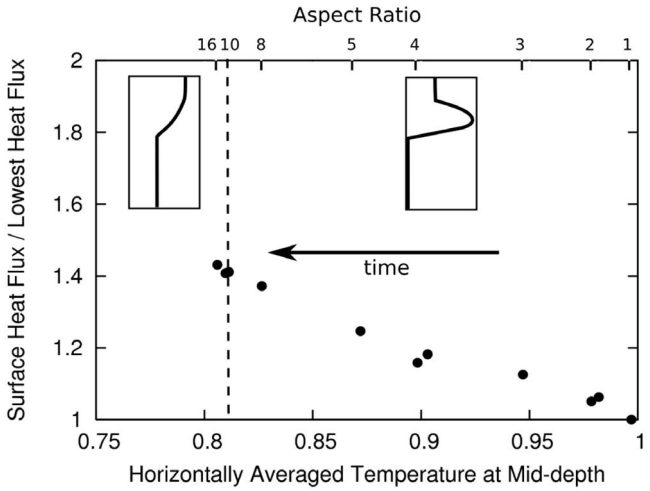

Figure 6. Internal temperature (horizontally averaged temperature at mid-depth) versus normalized surface heat flux for numerical simulations from *Höink and Lenardic* [2010]. Insets show schematic horizontal flow profiles for Couette flow at lower internal temperatures, in which sublithospheric flow is slower than plate velocities and cooling is efficient, and Poiseuille flow for higher internal temperatures, in which sublithospheric flow is faster than plate velocities. The transition occurs at internal temperatures close to 0.81. The time arrow indicates the direction of Earth's thermal evolution. The increasing trend suggests that convective heat loss was less efficient in Earth's hotter past, when sublithospheric flow exceed plate speeds, than in its cooler present state, in which large plates move faster than the asthenosphere.

at the transition aspect ratio (Figure 1c). In the short aspect ratio regime, in which sublithospheric flow exceeds plate speeds and internal mantle temperatures are high, surface heat flux increases with increasing aspect ratio, to a peak at the transition to the long aspect ratio regime, and subsequent comparatively gradual decline at higher aspect ratios. Figure 6 plots simulation results from Figures 2c and 2d of *Höink and Lenardic* [2010]. The surface heat flux–mantle temperature relation for the sluggish convection mode is different (surface heat flux increases with decreasing temperature) from mobile-lid convection (surface heat flux increases with increasing temperature). Different regimes have different scalings, because the driving mechanism and underlying planform of convection are different.

[52] Figure 7 shows examples of two thermal evolution models, one with a "classic" mobile-lid scaling [e.g., *Davies*, 1980], applicable for convection with a leading plate, and one with a sluggish-lid scaling derived from Figure 6, applicable for a flow configuration in which the asthenosphere leads the plate. Neither single scaling from these two different modes is able to explain Earth's thermal evolution alone. While the classic mobile-lid scaling allows for substantial heat loss and temperature drop during Earth's thermal evolution, it is unable to predict a present day Urey ratio (the ratio of radiogenic heat production to surface heat loss), that falls within the expected range [*Jaupart et al.*, 2007]. Constraining this scaling by the present day Urey ratio on the other hand leads to unrealistic high temperatures in Earth's past, often termed "thermal catastrophe" [e.g., *Korenaga*, 2008, and references therein]. In contrast, the sluggish-lid thermal history is able to limit heat loss in the past. However, this mechanism does not allow for significant cooling of Earth's mantle during its entire existence, leaving present day mantle temperatures unrealistically high. The inability of each scaling alone to provide a plausible thermal evolution for Earth's mantle is maybe not surprising if both modes operated during Earth's thermal evolution. A prediction from our work is that the thermal evolution of Earth's mantle can not be modeled with either of the two scalings alone. We propose that a regime transition over the Earth's history or a superposition of regimes has to be considered instead.

[53] In order to illustrate this point we present an example of the latter scenario here. Figure 8 shows a thermal evolution model for two different initial temperatures in which each of the scalings discussed above contributes equally to surface heat loss. This type of model simulates the co-existence of both types of convection, mobile-lid and sluggish-lid, at any given time during Earth's history, the same way the Pacific plate and the Atlantic plate co-exist at present. This model allows for

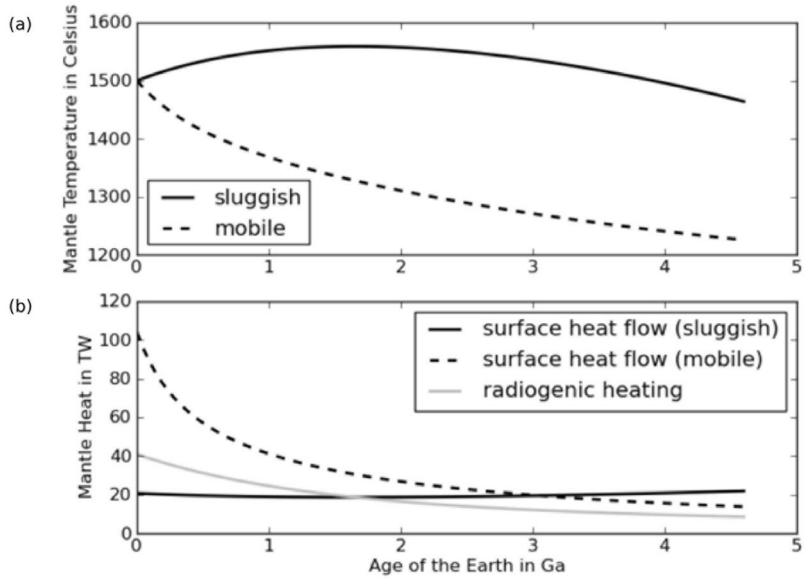

Figure 7. Examples of thermal evolution models for the mobile-lid scaling, using a classic scaling [e.g., *Davies*, 1980], and the sluggish-lid scaling, using a heat loss versus temperature scaling derived from Figure 6. Mobile-lid models are unable to capture the correct present day ratio of internal radiogenic heat input and surface heat loss (Urey ratio). Compared to mobile-lid scalings, sluggish-lid scalings limit heat loss in the past. However, a consequence are elevated temperatures which are maintained over long times due to the system's stiffness. The inability of either one scaling to produce a satisfactory thermal history, and the fact that both modes of convection operate over long time scales, renders it unlikely that a single heat loss–temperature scaling exists that can be used to model Earth's thermal history.

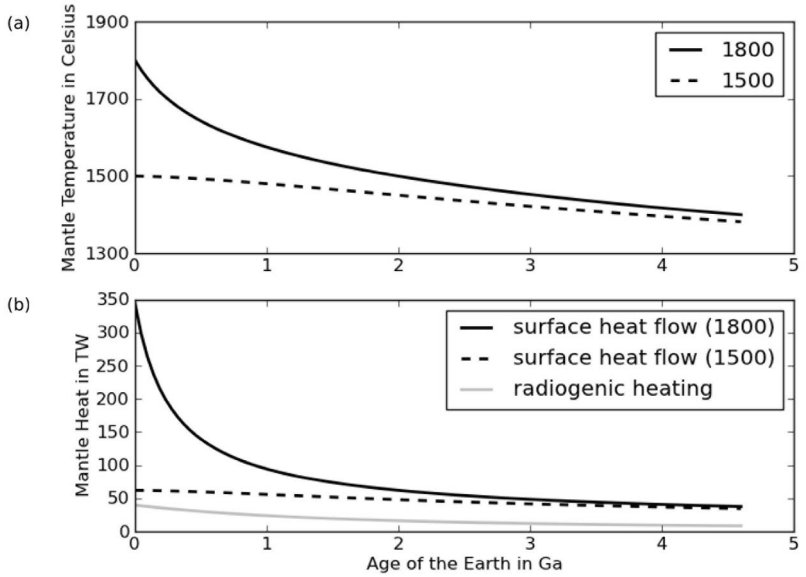

Figure 8. Examples of two thermal evolution models starting at different initial temperatures. In these models heat loss occurs to equal amounts from mobile-lid scaling, using a classic scaling [e.g., *Davies*, 1980], and the sluggish-lid scaling, using a heat loss versus temperature scaling derived from Figure 6. The combination of two heat loss scalings simulates the co-existence of different regimes at any given time, akin to the co-existence of Pacific plate and Atlantic plate at present. These types of models are able to loose an appropriate amount of heat early in Earth's history as to avoid overheating. At the same time they can capture a very low present day Urey ratio (0.24 and 0.22 for the models shown). One key ability of this type of model is, different from single-scaling models, that it allows for different initial conditions to reach both present day mantle temperature and Urey ratio, thus avoiding a "thermal catastrophe". The success of this simple two-mode model suggests an avenue for successfully modeling Earth's thermal history.

Table A1. Age-Binned Mean Shear Wave Velocity Minima Extracted From *Priestley and McKenzie* [2006] and *Gaherty and Dunn* [2007]

Region	V_s (km/s)	Age (Ma)	V_s (km/s)	Age (Ma)	V_s (km/s)	Age (Ma)	Source
Pacific	4.05	1	4.15	12	4.25	50	PM06
Pacific	4.00	2	4.18	12	4.23	36	GD07
Atlantic	4.08	7.5	4.14	17.5			GD07

cooling in the past, avoiding the sluggish-lid problem of elevated temperatures, while at the same time predicting a low present day Urey ratio, which solves a major problem of models that only use classic mobile-lid scaling. Recovering these two important characteristics allows this "two-mode" model to more successfully model Earth's thermal evolution than either end-member scaling alone. While Earth's thermal evolution was certainly influenced by other factors such as water-dependent rheology and continental coverage, the success of our simple two-mode model provides a new avenue for modeling Earth's thermal evolution, which we will pursue in the future.

9. Conclusion

[54] We have used scaling analyses to show that stress coupling at the lithosphere-asthenosphere boundary is the key to understanding how observed plate velocities are governed by dynamical contributions from plate subduction and from lateral flow in the asthenosphere. This coupling depends on the wavelength of convection and on the relative thicknesses and viscosities of the lithosphere and asthenosphere. An important result from this analysis is a prediction that the motions of small plates will be largely governed by flow in the asthenosphere, rather than by negative plate buoyancy (slab-pull) or ridge-push, in contrast to classical plate tectonic theory, which holds for large plates. For example, estimates of asthenosphere flow velocity ratios underneath Pacific plate and Atlantic plate suggest that the Pacific plate is driven mostly by subduction processes while the Atlantic plate is mostly driven by basal drag from strong asthenospheric flow. Resulting stress orientations are consistent with stress observations of North America. Lateral pressure gradients in the asthenosphere provide an explanation for the relatively smooth flanking topography at the East Pacific Rise compared to the steep flanking topography at the Mid Atlantic Ridge. Stress coupling at the base of the plate also provides a potential contribution to thermal history modeling studies which require a hotter Earth in the past to cool less efficiently than a cooler Earth at present day.

Appendix A: Converting Age-Binned Shear Wave Velocities to Temperature Gradients

[55] Table A1 lists age-binned mean shear wave velocities minima and average asthenosphere thicknesses from Pacific [*Priestley and McKenzie*, 2006; *Gaherty and Dunn*, 2007] and Atlantic [*Gaherty and Dunn*, 2007] regions. For the Atlantic region we choose the South Azores region because the seafloor bathymetry map shown by *Gaherty and Dunn* [2007] does not suggest a strong plume influence.

[56] When assuming that variations in shear wave velocity are primarily due to temperature differences, we can use the partial derivative $\partial \ln V_s/\partial T = -2.1\%/100\mathrm{K}$ [*Cammarano et al.*, 2003] to obtain temperature gradients using

$$\frac{\Delta T}{\Delta x} = \frac{\Delta T}{\Delta \mathrm{age}\, U} \tag{A1}$$

where U is the average plate velocity (1 cm/year for the Atlantic and 10 cm/year for the Pacific) and ΔT is given by

$$\Delta T = \Delta \ln V_s \left(\frac{\partial \ln V_s}{\partial T}\right)^{-1}. \tag{A2}$$

[57] The estimated temperature gradients are 50 K/100 km for the Atlantic. For the Pacific the estimates are 2 – 15 K/100 km (GD07) and 2 – 7 K/100 km (PM06), which averages to 7 K/100 km.

Acknowledgments

[58] We thank Peter Luffi for discussions, and John Sclater, Marcel Croon and anonymous reviewers for comments. TH was funded in part by NSF grant 0944156. AMJ acknowledges support from the Canadian Institute for Advanced Research and NSERC.

References

Adam, C., and V. Vidal (2010), Mantle flow drives the subsidence of oceanic plates, *Science*, *328*, 83–85.

Adam, C., and V. Vidal (2011), Response to comment on "Mantle flow drives the subsidence of oceanic plates," *Science*, *331*, 1011–1011.

Afrouz, A. (1992), *Practical Handbook of Rock Mass Classification Systems and Modes of Ground Failure*, CRC Press, Boca Raton, Fla.

Alvarez, W. (2010), Protracted continental collisions argue for continental plates driven by basal traction, *Earth Planet. Sci. Lett.*, *296*, 434–442.

Busse, F. H., M. A. Richards, and A. Lenardic (2006), A simple model of high Prandtl and high Rayleigh number convection bounded by thin low-viscosity layers, *Geophys. J. Int.*, *164*, 160–167.

Cammarano, F., S. Goes, P. Vacher, and D. Giardini (2003), Inferring upper-mantle temperatures from seismic velocities, *Phys. Earth Planet. Inter.*, *138*, 197–222.

Conrad, C. P., and C. Lithgow-Bertelloni (2002), How mantle slabs drive plate tectonics, *Science*, *298*, 207–209.

Croon, M. B., J. K. Hillier, and J. G. Sclater (2011), Comment on "Mantle flow drives the subsidence of oceanic plates," *Science*, *331*, 1011.

Dasgupta, R., and M. M. Hirschmann (2010), The deep carbon cycle and melting in Earth's interior, *Earth Planet. Sci. Lett.*, *298*, 1–13.

Davies, G. F. (1980), Thermal histories of convective earth models and constraints on radiogenic heat production in the Earth, *J. Geophys. Res.*, *85*, 2517–2530.

Davies, G. F., and M. A. Richards (1992), Mantle convection, *J. Geol.*, *100*, 151–206.

Dixon, J. E., T. H. Dixon, D. R. Bell, and R. Malservisi (2004), Lateral variation in upper mantle viscosity: Role of water, *Earth Planet. Sci. Lett.*, *222*, 451–467.

Doin, M. P., and L. Fleitout (1996), Thermal evolution of the oceanic lithosphere: An alternative view, *Earth Planet. Sci. Lett.*, *142*, 121–136.

Elsasser, W. M. (1967), Convection and stress propagation in the upper mantle, *Tech. Rep.*, *5*, Princeton Univ., Princeton, N. J.

Forsyth, D., and S. Uyeda (1975), On the relative importance of the driving forces of plate motion, *Geophys. J. R. Astron. Soc.*, *43*, 163–200.

Gaherty, J. B. (2001), Seismic evidence for hotspot-induced buoyant flow beneath the Reykjanes Ridge, *Science*, *293*, 1645–1647.

Gaherty, J. B., and R. A. Dunn (2007), Evaluating hot spot-ridge interaction in the Atlantic from regional-scale seismic observations, *Geochem. Geophys. Geosyst.*, *8*, Q05006, doi:10.1029/2006GC001533.

Griffiths, R. W. (1986), Thermals in extremely viscous fluids, including the effects of temperature-dependent viscosity, *J. Fluid Mech. Digital Arch.*, *166*, 115–138.

Gutenberg, B. (1959), *Physics of the Earth*'s *Interior*, Academic, New York.

Hager, B. H., and M. A. Richards (1989), Long-wavelength variations in Earth's geoid: Physical models and dynamical implications, *Philos. Trans. R. Soc. London, Ser. A Math. Phys. Sci.*, *328*, 309–327.

Hillier, J. K., and A. B. Watts (2004), "Plate-like" subsidence of the East Pacific Rise–South Pacific superswell system, *J. Geophys. Res.*, *109*, B10102, doi:10.1029/2004JB003041.

Hirschmann, M. M., P. D. Asimow, M. S. Ghiorso, and E. M. Stolper (1999), Calculation of peridotite partial melting from thermodynamic models of minerals and melts. III. Controls on isobaric melt production and the effect of water on melt production, *J. Petrol.*, *40*, 831–851.

Hirth, G., and D. L. Kohlstedt (1996), Water in the oceanic upper mantle: Implications for rheology, melt extraction and the evolution of the lithosphere, *Earth Planet. Sci. Lett.*, *144*, 93–108.

Höink, T., and A. Lenardic (2008), Three-dimensional mantle convection simulations with a low-viscosity asthenosphere and the relationship between heat flow and the horizontal length scale of convection, *Geophys. Res. Lett.*, *35*, L10304, doi:10.1029/2008GL033854.

Höink, T., and A. Lenardic (2010), Long wavelength convection, Poiseuille-Couette flow in the low-viscosity asthenosphere and the strength of plate margins, *Geophys. J. Int.*, *180*, 23–33.

Holmes, A. (1931), Radioactivity and Earth movements, *Geol. Soc. Glasgow Trans.*, *18*, 559–606.

Humphreys, E. D., and D. D. Coblentz (2007), North American dynamics and western U.S. tectonics, *Rev. Geophys.*, *45*, RG3001, doi:10.1029/2005RG000181.

Jaupart, C., S. Labrosse, and J.-C. Mareschal (2007), Temperatures, heat and energy in the mantle of the Earth, in *Treatise on Geophysics*, vol. 7, *Mantle Dynamics*, edited by D. Bercovici, pp. 253–304, Elsevier, Boston, Mass.

Jellinek, A. M., and M. Manga (2004), Links between long-lived hot spots, mantle plumes, d″, and plate tectonics, *Rev. Geophys.*, *42*, RG3002, doi:10.1029/2003RG000144.

Joseph, D. D. (1980), Boundary conditions for thin lubrication layers, *Phys. Fluids*, *23*, 2356–2358.

Korenaga, J. (2008), Urey ratio and the structure and evolution of Earth's mantle, *Rev. Geophys.*, *46*, RG2007, doi:10.1029/2007RG000241.

Lee, C.-T. A., A. Lenardic, C. M. Cooper, F. Niu, and A. Levander (2005), The role of chemical boundary layers in regulating the thickness of continental and oceanic thermal boundary layers, *Earth Planet. Sci. Lett.*, *230*, 379–395.

Lenardic, A., M. A. Richards, and F. H. Busse (2006), Depth-dependent rheology and the horizontal length scale of mantle convection, *J. Geophys. Res.*, *111*, B07404, doi:10.1029/2005JB003639.

Lin, J., and E. M. Parmentier (1989), Mechanisms of lithospheric extension at mid-ocean ridges, *Geophys. J.*, *96*, 1–22.

McKenzie, D. (1967), Some remarks on heat flow and gravity anomalies, *J. Geophys. Res.*, *72*, 6261–6273.

McKenzie, D. (1969), Speculations on the consequences and causes of plate motions, *Geophys. J. R. Astron. Soc.*, *18*, 1–32.

Mei, S., W. Bai, T. Hiraga, and D. L. Kohlstedt (1999), Influence of melt on the creep behavior of olivine-basalt aggregates under hydrous conditions, *Earth Planet. Sci. Lett.*, *201*, 491–507.

Moore, W. B. (2008), Heat transport in a convecting layer heated from within and below, *J. Geophys. Res.*, *113*, B11407, doi:10.1029/2006JB004778.

Morgan, J. P., and W. H. F. Smith (1992), Flattening of the sea-floor depth-age curve as a response to asthenospheric flow, *Nature*, *359*, 524–527.

Morgan, J. P., W. J. Morgan, Y.-S. Zhang, and W. H. F. Smith (1995), Observational hints for a plume-fed, suboceanic asthenosphere and its role in mantle convection, *J. Geophys. Res.*, *100*, 12,753–12,768.

O'Neill, C., A. M. Jellinek, and A. Lenardic (2007), Conditions for the onset of plate tectonics on terrestrial planets and moons, *Earth Planet. Sci. Lett.*, *261*, 20–32.

Parsons, B., and D. McKenzie (1978), Mantle convection and the thermal structure of the plates, *J. Geophys. Res.*, *83*, 4485–4496.

Parsons, B., and J. G. Sclater (1977), An analysis of the variation of ocean floor bathymetry and heat flow with age, *J. Geophys. Res.*, *82*, 803–827.

Paulson, A., and M. A. Richards (2009), On the resolution of radial viscosity structure in modelling long-wavelength postglacial rebound data, *Geophys. J. Int.*, *179*, 1516–1526.

Priestley, K., and D. McKenzie (2006), The thermal structure of the lithosphere from shear wave velocities, *Earth Planet. Sci. Lett.*, *244*, 285–301.

Richards, M. A., W.-S. Yang, J. R. Baumgardner, and H.-P. Bunge (2001), Role of a low-viscosity zone in stabilizing plate tectonics: Implications for comparative terrestrial planetology, *Geochem. Geophys. Geosyst.*, *2*(8), 1026, doi:10.1029/2000GC000115.

Richter, F. M. (1973), Dynamical models for sea floor spreading, *Rev. Geophys.*, *11*, 223–287.

Richter, F. M., and D. P. McKenzie (1978), Simple plate models of mantle convection, *J. Geophys.*, *44*, 441–471.

Schubert, G., D. Turcotte, and P. Olson (2001), *Mantle Convection in the Earth and Planets*, Cambridge Univ. Press, Cambridge, U. K.

Scott, T., and D. L. Kohlstedt (2006), The effect of large melt fraction on the deformation behavior of peridotite, *Earth Planet. Sci. Lett.*, *246*, 177–187.

Small, C. (1994), A global analysis of mid-ocean ridge axial topography, *Geophys. J. Int.*, *116*, 64–84.

Stein, C. A., and S. Stein (1994), Comparison of plate and asthenospheric flow models for the thermal evolution of oceanic lithosphere, *Geophys. Res. Lett.*, *21*, 709–712.

Thoraval, C., and M. A. Richards (1997), The geoid constraint in global geodynamics: Viscosity structure, mantle heterogeneity models and boundary conditions, *Geophys. J. Int.*, *131*, 1–8.

Turcotte, D. L., and E. R. Oxburgh (1967), Finite amplitude convective cells and continental drift, *J. Fluid Mech.*, *28*, 29–42.

Turner, J. (1979), *Buoyancy Effects in Fluids*, Cambridge Univ. Press, Cambridge, U. K.

Yamamoto, M., J. P. Morgan, and W. J. Morgan (2007a), Global plume-fed asthenosphere flow I: Motivation and model development, in *Plumes and Planetary Processes*, *Spec. Pap. Geol. Soc. Am.*, *430*, 165–188.

Yamamoto, M., J. P. Morgan, and W. J. Morgan (2007b), Global plume-fed asthenosphere flow II: Application to the geochemical segmentation of mid-ocean ridges, in *Plumes and Planetary Processes*, *Spec. Pap. Geol. Soc. Am.*, *430*, 189–208.